Journal of Thermal Analysis and Calorimetry, Vol 88 (2007) 3, 805–812

PRODUCTS AND KINETICS OF NON–ISOTHERMAL DECOMPOSITION OF VANADIUM(IV) OXIDE COMPOUNDS

L. T. Vlaev[*]*, V. G. Georgieva and S. D. Genieva*

Department of Physical Chemistry, Assen Zlatarov University, 8010 Bourgas, Bulgaria

The kinetics of dehydration and decomposition of $VOSO_4 \cdot 2H_2O$, $VOSO_4$ and $VOSeO_3 \cdot H_2O$ was studied under non-isothermal heating on a derivatograph. The stages and products of the thermal decomposition were determined. It was proved that $VOSO_4 \cdot 2H_2O$ decomposes to V_2O_5 while $VOSeO_3 \cdot H_2O$ – to V_2O_4. A number of kinetic models and calculation procedures were used to determine the values of the kinetic parameters characterizing the process. The parameters calculated were compared and analyzed. IR-spectra of the initial substances and the solid residue after decomposition are presented.

Keywords: *IR-spectra, non-isothermal kinetics, thermal decomposition, vanadium(IV) oxide selenite, vanadium(IV) oxide sulfate*

Introduction

According to some authors [1], only carbon forms more compounds than vanadium. This is a result of the variable degree of oxidation of vanadium (II, III, IV, V) and its ability to form stable complex cations (VO^{2+}, $V_2O_2^{4+}$, VO_2^{+}, VO^{3+} etc.), anions (VO_3^{-}, HVO_4^{2-}, VO_4^{3-} etc.), as well as complex ions. The considerable interest shown recently to vanadium compounds is due mainly to the fact that many of them have luminescent, magnetic and semi-conductor properties. A number of vanadium oxide compounds are known where vanadium is in either 4th or 5th degree of oxidation [3–18]. In this connection, $VOSO_4 \cdot nH_2O$ where n=2, 3, 3.5, 5 and 6.5 [1, 2] and $VOSeO_3 \cdot H_2O$ [7] are of special interest since, under heating in reduction medium (H_2 or CO), produce easily the corresponding sulfides and selenides. The latter also possess valuable semi-conductor properties. Besides, vanadium systems have been intensively studied for their coordination geometries, which lead to a great variety of potential polyhedral connectivities. The structures of inorganic solids containing selenite ion are very interesting because of the non-bonded electron pair that places the cation in the asymmetric coordination. From synthetic and crystal chemical perspective, it was suggested that there is rich structural chemistry in metal selenites. Examples of vanadium(IV) selenites $VOSeO_3 \cdot H_2O$, AV_2SeO_7 (A=K and Rb) and $Ba(VO)_2(SeO_3)_2(HSeO_3)_2$ which show dimmer, one dimensional antiferromagnetic, and no magnetic couplings, respectively were discussed in the literature. $VOSeO_3$ and $VOSe_2O_5$ were also reported [7, 14]. However, no data on the thermal stability, mechanism of decomposition under heating and the kinetics of this process were found in the available literature.

The aim of the present work is to study the mechanism and kinetics of decomposition of $VOSO_4 \cdot 2H_2O$ and $VOSeO_3 \cdot H_2O$ under non-isothermal heating, as well as the composition of the products obtained.

Experimental

Materials and measurements

The objects studied were $VOSO_4 \cdot 2H_2O$ (Riedel-de Haën) and $VOSeO_3 \cdot H_2O$. The latter was synthesized by mixing solutions of $VOSO_4$ and Na_2SeO_3 at room temperature and pH=5.5. The precipitate obtained was filtered, washed with distilled water and dried in air at 373 K for 6 h. According to the data obtained from chemical and X-ray powder analysis, the substance could be described by the formula: $VOSeO_3 \cdot H_2O$. Anhydrous $VOSO_4$ was prepared by heating $VOSO_4 \cdot 2H_2O$ in air at 540 K for 6 h.

The thermo-gravimetrical measurements were carried out in a flow of nitrogen at a rate of 20 cm^3 min^{-1} under non-isothermal conditions in a derivatograph system Paulik–Paulik–Erdey (MOM, Hungary) at heating rate of 10 K min^{-1} up to 1123 K. Samples of 100 mg were weighted into a 7 mm diameter 14 mm high platinum crucible, without pressing. α-Aluminina calcined up to 1373 K was used as a standard reference

* Author for correspondence: vlaev@btu.bg

1388–6150/$20.00

Akadémiai Kiadó, Budapest, Hungary
Springer, Dordrecht, The Netherlands

material. The TG, DTA and DTG curves were recorded graphically with 1 mg sensitivity.

The IR absorption spectra were taken over the region from 400 to 4000 cm^{-1} (resolution 1 cm^{-1}) on a Specord – 75 spectrophotometer (Carl Zeiss, Jena, Germany) The experiments were carried out at room temperature using KBr pellets with concentration of the substance studied 0.3 mass%.

Theoretical background

Decompositions of the compounds is a solid–state process of the type:

$$A(solid) \rightarrow B(solid)+C(gas)$$

The kinetics of such reactions is described by various equations taking into account the special features of their mechanisms. The calculation of kinetic data is based on the following equation:

$$g(\alpha)=\frac{A}{q}\int_0^T e^{-E/RT}dT \quad (1)$$

where α – decomposed fraction, q – heating rate, E – activation energy, A – pre-exponential factor, T – sample temperature, R – gas constant. The first term of Eq. (1) is easy to solve [19–23]. Their algebraic expressions are presented in Table 1. The integral of the exponential does not present an exact analytical solution; even so, various approximations for the calculation of this integral have been proposed, originating from different methods for the calculation of kinetic parameters.

The kinetics parameters can be derived using a modified Coats–Redfern equation [24]:

$$\ln\frac{g(\alpha)}{T^2}=\ln\frac{AR}{qE}-\frac{E}{RT} \quad (2)$$

where $g(\alpha)$ is a function, the expression of which depends on the kinetics model of the occurring reaction, presented in Table 1.

Tang *et al.* [25] propose new approximate formula for Arrhenius temperature integral, which give a next linear equation:

$$\ln\left[\frac{g(\alpha)}{T^{1.894661}}\right]=\left[\ln\frac{AE}{qR}+3.63504095-1.894661\ln E\right]-1.00145033\frac{E}{RT} \quad (3)$$

Wanjun *et al.* [26] propose another approximate formula for Arrhenius temperature integral, which give a next linear equation:

$$\ln\left[\frac{g(\alpha)}{T^2}\right]=\ln\left[\frac{AR}{q(1.00198882E+1.87391198RT)}\right]-\frac{E}{RT} \quad (4)$$

The values of the activation energy E and the pre-exponential factor A in Arrhenius equation can be calculated from the slope and cut-off on the ordinate axes. If the correct $g(\alpha)$ is used, a plot of $\ln[g(\alpha)/T^2]$ *vs.* $1/T$ should give a straight line with the highest correlation coefficient at the linear regression analysis. It is well known, that the formal expressions of the functions $g(\alpha)$ depend on the conversion mechanism and its mathematical model [19–23]. The latter usually represents the limiting stage of the reaction – the chemical reactions; random nucleation and nuclei growth; phase boundary reaction or diffusion. Table 1 shows the most common kinetics models and their algebraic expressions [20, 22, 27].

The other kinetics parameters of the process can be calculated using the fundamental theory of the activated complex (transition state) and Eyring equation [26, 27]

$$k=\frac{e\chi k_B T}{h}\exp\left(\frac{\Delta S^{\neq}}{R}\right)\exp\left(-\frac{E}{RT}\right) \quad (5)$$

where χ is the transition factor, which is unity for monomolecular reaction, k_B is the Boltzmann constant, h is the corresponding Plank constant, e=2.7183 is the Neper number and $\Delta S^{\neq}$ is the change of entropy for the activated complex formation from the reagent.

Taking into account Eq. (5) and the pre-exponential factor from the Arrhenius equation, the following expression is obtained:

$$A=\frac{e\chi k_B T}{h}=\exp\left(\frac{\Delta S^{\neq}}{R}\right) \quad (6)$$

and $\Delta S^{\neq}$ can be calculated according to the formula:

$$\Delta S^{\neq}=R\ln\frac{Ah}{e\chi k_B T_P} \quad (7)$$

where T_p is the peak temperature from the DTG curve. Since

$$\Delta H^{\neq}=E-RT \quad (8)$$

the change of the enthalpy $\Delta H^{\neq}$ and Gibbs free energy $\Delta G^{\neq}$ for the activated complex can be calculated using the well known thermodynamic equation [27]:

$$\Delta G^{\neq}=\Delta H^{\neq}-T\Delta S^{\neq} \quad (9)$$

$\Delta S^{\neq}$, $\Delta H^{\neq}$ and $\Delta G^{\neq}$ were calculated at T=T_p, since this temperature characterizes the highest rate of the process and, therefore, is the important parameter.

Table 1 Algebraic expressions of $f(\alpha)$ and $g(\alpha)$ for the kinetic models of thermal decomposition, considered in this work

Symbol	$f(\alpha)=\alpha^m(1-\alpha)^n[-\ln(1-\alpha)]^p$	$g(\alpha)=\int_0^\alpha \frac{d\alpha}{f(\alpha)}=kt$	Reaction model
1. Chemical decomposition process or mechanism non-invoking equations			
$F_{3/2}$	$(1-\alpha)^{3/2}$	$2[(1-\alpha)^{-1/2}-1]$	Three-halves order kinetics
F_2	$(1-\alpha)^2$	$\alpha/(1-\alpha)$	Second-order kinetics
F_n	$(1-\alpha)^n$	$[1-(1-\alpha)^{1-n}]/(1-n)$	n^{th} order kinetics ($n\neq1$)
2. Acceleratory rate equations			
$P_{3/2}$	$\alpha^{-1/2}$	$(2/3)\alpha^{3/2}$	Power law ($\alpha=kt^{2/3}$)
P_2	$\alpha^{1/2}$	$2\alpha^{1/2}$	Power law ($\alpha=kt^2$)
P_3	$\alpha^{2/3}$	$3\alpha^{1/3}$	Power law ($\alpha=kt^3$)
P_4	$\alpha^{3/4}$	$4\alpha^{1/4}$	Power law ($\alpha=kt^4$)
P_5	α	$\ln\alpha$	Exponential law ($\alpha=1-\exp(-kt)$
3. Sigmoid rate equations or random nucleation and subsequent growth			
A_1, F_1	$1-\alpha$	$-\ln(1-\alpha)$	Random nucleation or first order kinetics
$A_{3/2}$	$(1-\alpha)[-\ln(1-\alpha)]^{1/3}$	$(3/2)[-\ln(1-\alpha)]^{2/3}$	Avrami – Erofe'ev Eq. (n=1.5)
A_2	$(1-\alpha)[-\ln(1-\alpha)]^{1/2}$	$2[-\ln(1-\alpha)]^{1/2}$	Avrami – Erofe'ev Eq. (n=2)
A_3	$(1-\alpha)[-\ln(1-\alpha)]^{2/3}$	$3[-\ln(1-\alpha)]^{1/3}$	Avrami – Erofe'ev Eq. (n=3)
A_4	$(1-\alpha)[-\ln(1-\alpha)]^{3/4}$	$4[-\ln(1-\alpha)]^{1/4}$	Avrami – Erofe'ev Eq. (n=4)
A_u	$\alpha(1-\alpha)$	$\ln[\alpha/(1-\alpha)]$	Prout – Tompkins Eq.
4. Deceleratory rate equations			
4.1. Phase boundary reaction			
R_1, P_1, F_0	$(1-\alpha)^0$	α	One dimensional advance of the reaction interface, power law ($\alpha=kt$) or zero order kinetics
R_2, $F_{1/2}$	$(1-\alpha)^{1/2}$	$2[1-(1-\alpha)^{1/2}]$	Contracting area (cylindrical symmetry) or one-half order kinetics
R_3, $F_{2/3}$	$(1-\alpha)^{2/3}$	$3[1-(1-\alpha)^{1/3}]$	Contracting volume (spherical symmetry) or two-thirds order kinetics
4.2. Based on the diffusion mechanism			
D_1	$1/\alpha$	$\alpha^2/2$	One dimensional diffusion or parabolic law ($\alpha=kt^{1/2}$)
D_2	$1/-\ln(1-\alpha)$	$\alpha+(1-\alpha)\ln(1-\alpha)$	Two dimensional diffusion (Valensi equation)
D_3	$(1-\alpha)^{2/3}/1-(1-\alpha)^{1/3}$	$(3/2)[1-(1-\alpha)^{1/3}]^2$	Three dimensional diffusion (Jander equation)
D_4	$(1-\alpha)^{1/3}/1-(1-\alpha)^{1/3}$	$(3/2)[1-(2/3)\alpha-(1-\alpha)^{2/3}]$	Three dimensional diffusion (Ginstling–Brounshtein equation)
D_5	$(1-\alpha)^{5/3}/1-(1-\alpha)^{1/3}$	$(3/2)[(1-\alpha)^{-1/3}-1]^2$	Zuravlev–Lesokhin–Tempelman equation
D_6	$(1+\alpha)^{2/3}/[(1+\alpha)^{1/3}-1]$	$(3/2)[(1+\alpha)^{1/3}-1]^2$	Komatsu–Uemura or anti-Jander equations

Results and discussion

Figure 1 shows the TG, DTA and DTG curves of the dehydration and decomposition of $VOSO_4{\cdot}2H_2O$, $VOSO_4$ and $VOSeO_3{\cdot}H_2O$.

As can be seen from Fig. 1 (curves 1), the TG-curves formed three clearly distinguishable steps while the DTA curves showed three endothermic effects at 423, 538 and 873 K respectively. The results from the thermogravimetric analysis (the mass loss recorded in the TG curve) and the calculations made with them were considered enough to suggest a step-wise mechanism of dehydration and decomposition of $VOSO_4{\cdot}2H_2O$, involving the following stages:

$$VOSO_4{\cdot}2H_2O \rightarrow VOSO_4+2H_2O \quad \text{Stage I}$$

$$2VOSO_4 \rightarrow V_2O_4(SO_4)+SO_2 \quad \text{Stage II}$$

$$V_2O_4(SO_4) \rightarrow V_2O_5+SO_2+1/2O_2 \quad \text{Stage III}$$

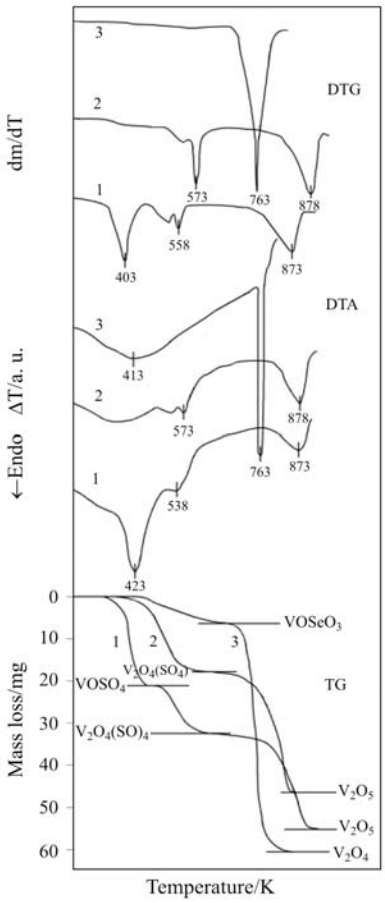

Fig. 1 TG, DTA and DTG curves of the samples: 1 – $VOSO_4 \cdot 2H_2O$; 2 – $VOSO_4$ and 3 – $VOSeO_3 \cdot H_2O$

Stages II and III were assumed to occur on the bases of both chemical analysis and the mechanism of thermal decomposition of other sulfates like $NiSO_4$ and $FeSO_4$ described in [22, 28]. Besides, the data from the chemical and X-ray powder diffraction analyses of the residual solid phase showed that it was V_2O_5. The chemical analysis shows 55.8 mass% contents of vanadium in solid residue in the third stage.

The TG curve (curve 2) registered by thermal treatment of $VOSO_4$ showed two steps and the DTA curve showed two endothermic effects at 573 and 878 K. They correspond to the decompositions at stages II and III.

Similarly, the TG curve taken by thermal treatment of $VOSeO_3 \cdot H_2O$ (curve 3) had two steps and the DTA curve – two endothermic effects at 413 and 763 K. The first effect was attributed to the release of crystallization water and the second effect – decomposition according to the following scheme:

$$VOSeO_3 \cdot H_2O \rightarrow VOSeO_3 + H_2O \qquad \text{Stage I}$$

$$2VOSeO_3 \rightarrow V_2O_4 + 2SeO_2 \qquad \text{Stage II}$$

The chemical analysis of solid residue from the second stage of decomposition shows 61.2 mass% vanadium content. The X-ray powder diffraction analyses of $VOSO_4$ and $VOSeO_3$ give patterns, characteristic for V_2O_5 and V_2O_4 respectively. This mean that the decomposition of $VOSO_4$ involves intramolecular oxy-reduction transformation while the decomposition of $VOSeO_3$ takes place without change of vanadium and selenium degree of oxidation.

On Fig. 2 are presented the IR spectra of the initial samples and final products.

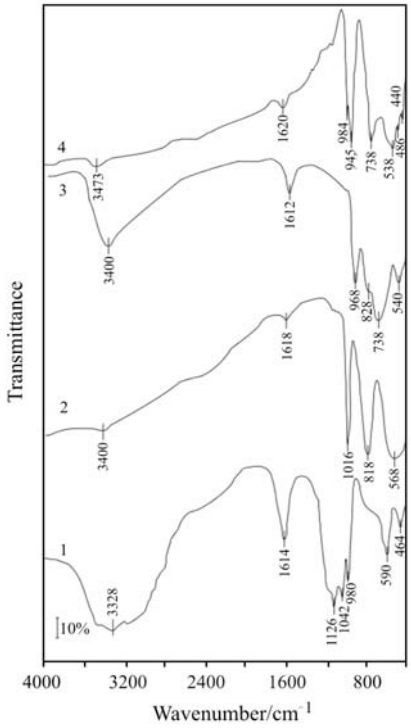

Fig. 2 IR spectra of: 1 – $VOSO_4 \cdot 2H_2O$; 2 – V_2O_5; 3 – $VOSeO_3 \cdot H_2O$ and 4 – V_2O_4

As can be seen from Fig. 2, wide absorption bands corresponding to stretching vibrations of OH-groups in the molecules of the crystallization water were registered in the high frequency region. The band in the IR-spectrum of $VOSeO_3 \cdot H_2O$ with maximum at 3400 cm^{-1} was narrower but the same band in the spectrum of $VOSO_4 \cdot 2H_2O$ is composite and, therefore, is quite wider. The reason for this is in the fact that the two water molecules are not in equivalent positions; hence they are not energetically equal according to the scheme [28]:

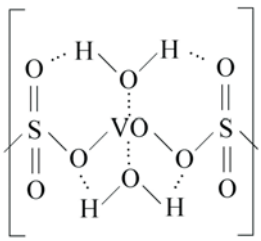

This was confirmed by the different intensity of the bands at 1616–1620 cm^{-1}. They are due to deformation vibrations of water molecules in $VOSO_4 \cdot 2H_2O$ and $VOSeO_3 \cdot H_2O$. In the spectra of V_2O_5 and V_2O_4 (spectra 2 and 4) however, bands with such frequencies were not observed because both oxides are not hygroscopic and do not absorb moisture from the atmosphere.

The absorption bands observed in the low frequency region of the IR-spectrum (1200–400 cm^{-1}) are due to the characteristic absorption bands of SO_4 and SeO_3 groups and V–O bonds. It should be noted for $VOSeO_3 \cdot H_2O$ that this group of bands was observed at frequencies lower by about 380 cm^{-1} compared to $VOSO_4 \cdot 2H_2O$. It can be explained with the higher mass of the SeO_3 group compared to SO_4. For clarity, a scheme of SeO_3^{2-} with angles and bond lengths between the atoms, as well as a scheme of $VOSeO_3$, are shown below. Table 2 shows the absorption bands of SeO_3^{2-} anion and its assignment [29–37].

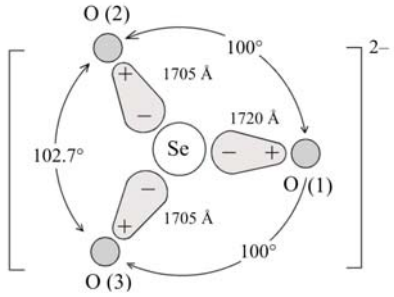

Scheme of SeO_3^{2-} anion

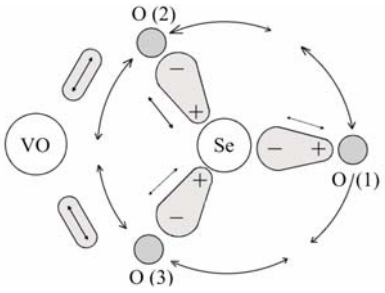

Scheme of $VOSeO_3$

It can be seen from the first scheme that the electron density of oxygen atoms in selenite anion is pulled to the selenium atom compared to the isolated O^{2-} ion. The second scheme shows that, due to the effect of anion counterpolarization under the influence of the anion, the electron density of the bond O–Se is pulled towards the positive charge [38]. Depending on cation nature and its polarizing ability, the degree of the counterpolarization effect is different which results in different vibration frequencies of the corresponding bonds. For instance, the shoulder at 828 cm^{-1} is due to the symmetric stretching vibrations of the Se–O bond(1) while the high intensity band with absorption maximum at 738 cm^{-1} – to the superposition of symmetric and asymmetric stretching vibrations of the Se–O(2,3) bonds with these of the V–O bond. These considerations were confirmed from the bands observed in the IR spectrum of V_2O_4 (spectrum 4). This spectrum was substantially different from that of V_2O_5 (spectrum 2). Thus, it was once again confirmed that the residual product from the thermal decomposition of $VOSO_4$ is V_2O_5 while that of the decomposition of $VOSeO_3$ is V_2O_4. It means that change of the degree of oxidation was observed neither for vanadium, nor selenium while during the decomposition of $VOSO_4$ the oxidation stage changed from +4 to +5 and that of sulfur – from +6 to +4 and the process occurred with release of oxygen according to stage III. The same mechanism was proposed for thermal decomposition of $NiSO_4$ [21].

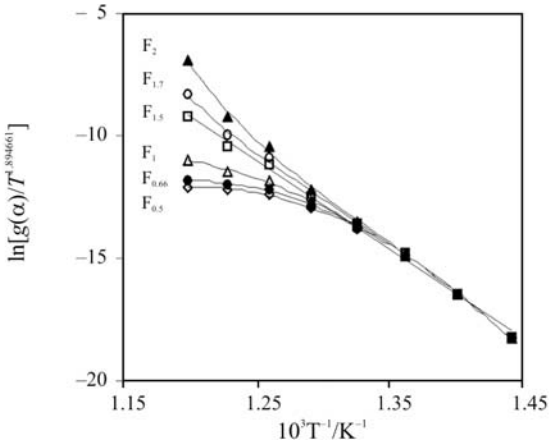

Fig. 3 Kinetic curves of thermal decomposition of $VOSeO_3$ at different kinetic equations

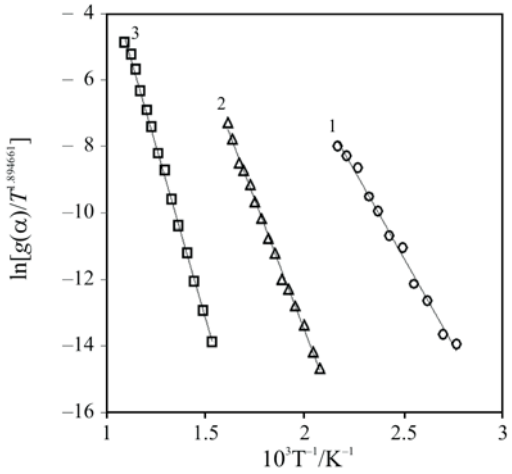

Fig. 4 Kinetic curves of thermal decomposition of $VOSO_4 \cdot 2H_2O$: 1 – stage I, 2 – stage II and 3 – stage III

Using the corresponding TG curves, the calculation procedures of Coats and Redfern [24], Tang *et al.* [25] and Wanjun *et al.* [26], as well as the algebraic expressions for $g(\alpha)$ presented in Table 1, the calculations were performed and the results obtained for the values of the activation energy E and pre-exponential factor in Arrhenius equation were compared. The comparison showed minimal differences between the results from the different methods used but the procedure of Tang *et al.* [25] was preferred. The values of the correlation coefficient of linear regression R^2, however, were found to depend strongly on the type of the selected $g(\alpha)$ function. Besides, the so-called mechanism non-invoking equations (Table 1) turned out to be the most suitable in this case. This is illustrated by the kinetic curves of thermal decomposition of $VOSeO_3$ obtained at different values of n, presented on Fig. 3.

The kinetic model for given stage was established on the base of the best values of the correlation coefficient R^2. Figure 3 shows that linear dependence with maximum value of correlation coefficient R^2 can be obtained at n=1.5. The TG curves characterizing the thermal decomposition of $VOSO_4 \cdot 2H_2O$ and $VOSO_4$ were processed by the same way. The kinetic curves of dehydration and decomposition of $VOSO_4 \cdot 2H_2O$ along the three steps of the TG curve are presented in Fig. 4.

Table 2 IR absorption bands SeO_3^{2-} and its assignment

Symbol	Assignment	Frequency/cm^{-1}
ν_1(A')	SeO(1) sysm. stretch	800
ν_2(A')	O(2)–Se–O(3) sym. bend	450
ν'_3(A')	Se–O(2,3) sym. stretch	670
ν''_3(A")	Se–O(2,3) asym. stretch	660
ν'_4(A')	Se–O(1,2,3) sym. deformation	335
ν''_3(a")	Se–O(1,2,3) asym. deformation	375

The kinetic curves shown in Fig. 4 had maximal correlation coefficients R^2 but they were obtained with different values of n. For instance, for the first stage n=1.5, for the second one – n=1.0 and for the

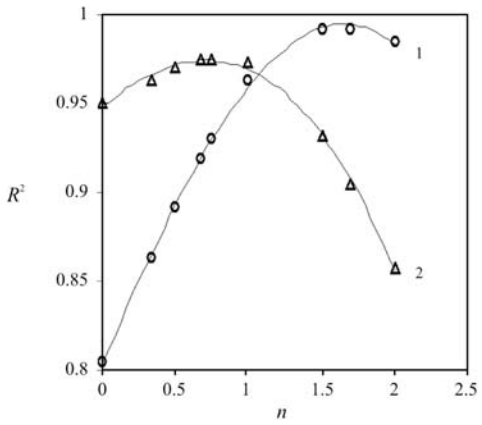

Fig. 5 Dependence of the coefficient of linear regression R^2 the values of n for: decomposition of 1 – $VOSO_4$ to $V_2O_4(SO_4)$ and 2 – $V_2O_4(SO_4)$ to V_2O_5

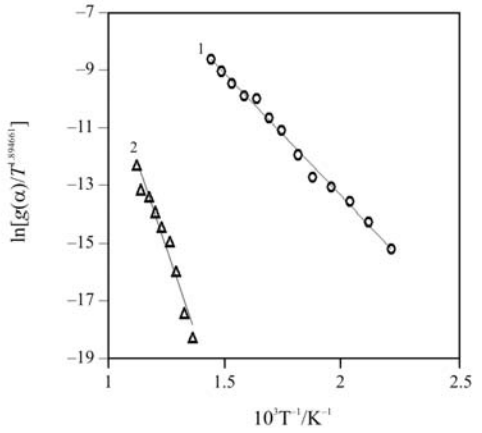

Fig. 6 Kinetic curves of thermal decomposition of 1 – $VOSO_4$ to $V_2O_4(SO_4)$ and 2 – $V_2O_4(SO_4)$ to V_2O_5

Table 3 Kinetic characteristics of non-isothermal decomposition of some vanadium(IV) oxide compounds, calculated according Tang *et al.* procedure [25]

Parameter	$VOSO_4 \cdot 2H_2O$			$VOSO_4$		$VOSeO_3 \cdot H_2O$	
	Stage I	Stage II	Stage III	Stage II	Stage III	Stage I	Stage II
Mechanism	$F_{1.5}$	$F_{1.0}$	$F_{0.5}$	$F_{1.65}$	$F_{0.5}$	$F_{2.0}$	$F_{1.5}$
R^2	0.9927	0.9974	0.9994	0.9947	0.9894	0.9929	0.9965
E/kJ mol^{-1}	88.2	129.4	183.7	70.4	188.2	58.5	303.0
A/min^{-1}	$2.16 \cdot 10^{11}$	$3.46 \cdot 10^{12}$	$6.35 \cdot 10^{12}$	$1.72 \cdot 10^{6}$	$7.17 \cdot 10^{12}$	$8.57 \cdot 10^{4}$	$2.12 \cdot 10^{20}$
T_p/K	423	538	873	573	878	413	763
$-\Delta S^{\neq}$/J mol^{-1} K^{-1}	73.2	52.1	51.1	173.3	50.1	195.5	–94.1
$\Delta H^{\neq}$/kJ mol^{-1}	84.7	124.9	176.4	65.6	180.9	55.1	296.7
$\Delta G^{\neq}$/kJ mol^{-1}	115.6	153.0	221.0	165.5	224.9	135.8	224.9

*$\Delta S^{\neq}$, $\Delta H^{\neq}$ and $\Delta G^{\neq}$ are calculated of the peak temperature T_p

third – n=0.5; i.e. there was a tendency of decrease of the value of n with the increase of the temperature of the corresponding stage. The same tendency was observed for the thermal decomposition of the anhydrous $VOSO_4$. Therefore, the dependence of the values of correlation coefficient of linear regression R^2 on the value of the parameter n are shown in Fig. 5.

As can be seen from Fig. 5 that maximum R^2 values were obtained at different values of n for the different stages. For instance, for the decomposition of $VOSO_4$ to $V_2O_4(SO_4)$ n=1.65 while for the decomposition of $V_2O_4(SO_4)$ to V_2O_5 n=0.50. Figure 6 shows the kinetic curves for the different stages.

Obviously, the slopes and the cut-offs are different which implies that the kinetic parameters characterizing the two stages would also be quite different. This was confirmed by the values of the parameters characterizing the kinetics of thermal decomposition of the different compounds and stages presented in Table 3.

It can be seen from the data on the thermal decomposition of $VOSO_4 \cdot 2H_2O$ shown in Table 3 that the higher is the temperature at which the stage occurs the smaller are the values of n and the higher are the values of E and A. The same tendency was observed for the thermal decomposition of $VOSO_4$. The higher values of E and A for the decomposition of $VOSO_4 \cdot 2H_2O$ at stage II (129.4 kJ mol^{-1}) compared to the same stage of the decomposition of the anhydrous $VOSO_4$ (70.4 kJ mol^{-1}) were considered to be due to fact that in the first case stage II overlaps stage I; thus, the structure of the forming anhydrous $VOSO_4$ is still in process of rearrangement while in the second case it had reached its equilibrium state. The decomposition during stage III for both $VOSO_4 \cdot 2H_2O$ and $VOSO_4$ showed almost equal values of the parameters n, E and A since, in both cases, stage two began after the end of stage I.

The thermal decomposition of $VOSeO_3 \cdot H_2O$ proceeded in two stages – first dehydration and second – decomposition with release of SeO_2 and formation of solid residue of V_2O_4. It has been reported [39] that at values of E lower than 100 kJ mol^{-1} the processes occur under diffusion control. Therefore, the water molecules in the crystallohydrates $VOSO_4 \cdot 2H_2O$ and $VOSeO_3 \cdot H_2O$ are weakly bonded to the crystal lattice. This was confirmed from the slightly higher temperatures of dehydration.

The significantly higher values of E and A observed for the thermal decomposition of $VOSeO_3 \cdot H_2O$ compared to these of $VOSO_4 \cdot 2H_2O$ showed that the bond strength between VO^{2+} and SeO_3^{2-} ions was higher than that between VO^{2+} and SO_4^{2-} ions. This was sustained by the different values of the change of entropy $\Delta S^{\neq}$ for the formation of the activated complex of the reagent. According to [39], the negative values of $\Delta S^{\neq}$ indicate that the activated complex has a more ordered structure than the reactant and that the reaction is 'slower' than normal. The values of $\Delta S^{\neq}$ for all stages of dehydration and decomposition of $VOSO_4 \cdot 2H_2O$ and $VOSO_4$ were found to be negative while for $VOSeO_3 \cdot H_2O$ they were negative for the dehydration and positive for the decomposition. The latter can be interpreted as a proof that the structure of $VOSeO_3$ was more ordered than the activated complex. Besides, the decomposition of $VOSeO_3$ did not involve change of vanadium and selenium degrees of oxidation, unlike $VOSeO_3$. It should be noted also that the higher are the values of E and A, the higher are the values of $\Delta S^{\neq}$. Similar tendencies were observed from other authors [40], although by thermal decomposition of other compounds.

Conclusions

Based on the studies carried out, the thermal decomposition of $VOSO_4 \cdot 2H_2O$ and $VOSeO_3 \cdot H_2O$ was found to proceed by different schemes. The first compound decomposes in three stages, while the second one – in two stages. The decomposition of $VOSO_4$ to V_2O_5 involves intramolecular oxy-reduction transformation while the decomposition of $VOSeO_3$ to V_2O_4 takes place without change of vanadium and selenium degree of oxidation. The parameters characterizing the kinetics of thermal decomposition of both salts were different because the nature of the cation exerts significant effect on electron density and hence, on the strength of its bond to the anion. Therefore, the thermal dissociation of $VOSO_4$ proceeds in two stages while that of $VOSeO_3$ – in one stage.

References

1 V. N. Muzgin, L. B. Hamzina, V. L. Zolotavin and I. Ya. Bezrukov, Analiticheskaya khimiya vanadiya, Nauka, Moscow, 1981.
2 R. Ripan and I. Chetyanu, Neorganicheskaya Khimiya, vol. 2, Mir, Moscow, 1972.
3 G. Meunier, M. Bertaund and J. Galy, Acta Crystallogr. B30 (1974) 2834.
4 J. C. J. Bart and G. Petrini, Z. Anorg. Allg. Chem., 422 (1976) 179.
5 J. C. Trombe, A. Gleizes and J. Galy, C. R. Acad. Sci. Ser. 2, 297 (1983) 667.
6 J. C. Trombe, A. Gleizes, J. Galy and J. P. Renard, Y. Journaux, New J. Chem., 11 (1987) 331.
7 G. Huan, J. W. Johnson, A. J. Jacobson, D. P. Goshorn and J. S. Merola, Chem. Mater., 3 (1991) 539.

8 W. T. A. Harrison, J. T. Vaughey, A. J. Jacobson, D. P. Goshorn and J. W. Johnson, J. Solid State Chem., 116 (1995) 77.
9 K. S. Lee, Y. U. Kwon, Y. U. Kwon, H. Namgung and S. H. Kim, Inorg. Chem., 34 (1995) 4178.
10 W. T. A. Harrison, L. L. Dussac and A. J. Jacobson, Acta Crystallogr., Section C, 51 (1995) 24.
11 Y. H. Kim, Y. U. Kwon and K. S. Lee, Bull. Korean Chem. Soc., 17 (1996) 1123.
12 K. S. Lee and Y. U. Kwon, J. Korean Chem. Soc., 40 (1996) 379.
13. Y. U. Kwon, K. S. Lee and Y. H. Kim, Inorg. Chem., 35 (1996) 1161.
14 Y. H. Kim, K. S. Lee and Y. U. Kwon, Inorg. Chem., 35 (1996) 7394.
15 P. S. Halasyamani and D. O'Hare, Inorg. Chem., 36 (1997) 6409.
16 V. P. Verma, Thermochim. Acta, 327 (1999) 63 and references therein.
17 W. T. A. Harrison, Acta Cryst., Section C, 56 (2000) 422.
18 Y. T. Kim, Y. H. Kim, K. Park and Y. U. Kwon, J. Solid State Chem., 161 (2001) 23.
19 J. Šestak and G. Berggren, Thermochim. Acta, 3 (1971) 1.
20 C. L. Albano, R. Sciamanna, T. Aquino and J. Martinez, European Congress on Computational Methods in Applied Sciences and Enginering, (ECCOMAS 2000, Barcelona, 11–14 September 2000).
21 E. Tomaszewicz and M. Kotfica, J. Therm. Anal. Cal., 77 (2004) 25.
22 L. T. Vlaev, V. G. Georgieva and G. G. Gospodinov, J. Therm. Anal. Cal., 79 (2005) 163.
23 T. Wanjun, L. Yuwen, Y. Xil, W. Zhiyong and W. Cunxin, J. Therm. Anal. Cal., 81 (2005) 347
24 W. Coats and J. P. Redfern, Nature (London) 201, (1964) 68.
25 W. Tang, Y. Liu, H. Zang and C. Wang, Thermochim. Acta, 408 (2003) 39.
26 T. Wanjun, L. Yuwen, Z. Hen, W. Zhiyong and W. Cunxin, J. Therm. Anal. Cal., 74 (2003) 309.
27 L. T. Vlaev, I. G. Markovska and L. A. Lyubchev, Thermochim. Acta, 406 (2003) 1.
28 V. P. Verma and A. Khushu, J. Thermal Anal., 35 (1989) 1157.
29 L. T. Vlaev, S. D. Genieva and V. G. Georgieva, J. Therm. Anal. Cal., 86 (2006) 449.
30 L. T. Vlaev, S. D. Genieva and G. G. Gospodinov, J. Therm. Anal. Cal., 81 (2005) 469.
31 K. I. Petrov, I. V. Tananaev, A. N. Volodina and N. K. Bol'shakova, Zh. Neorg. Khim., 22 (1977) 1453.
32 R. Ya. Melnikovskii, V. N. Makatun and V. V. Pechkovskii, Zh. Neorg. Khim., 19 (1974) 1864. (in Russian).
33 R. C. Cody, Levitt, R. S. Viswanath and P. J. Miller, J. Solid State Chem., 26 (1978) 281.
34 M. Ebert, Z. Mička and I. Pekova, Chem. Zvesti, 36 (1982) 169.
35 M. Ebert, Z. Mička and I. Pekova, Collect. Czech. Chem. Commun., 47 (1982) 2069.
36 G. G. Gospodinov, L. M. Sukhova and K. I. Petrov, Zh. Neorg. Khim., 33 (1988) 1970 (in Russian).
37 P. P. Pradyumnan and M. A. Ittyachen, J. Therm. Anal. Cal., 61 (2000) 243.
38 L. I. Martynenko and V. I. Spitzin, Metodicheskie aspekty kursa neorganicheskoi khimii, Moscow University, Moscow, 1983, (in Russian).
39 A. A. Frost and R. G. Pearson, Kinetics and Mechanism of Chemical Reactions, John Wiley and Sons Inc., New York, 1961.
40 L. K. Singh and S. Mitra, Thermochim. Acta, 138 (1989) 285.

Received: June 30, 2006
Accepted: December 28, 2006
OnlineFirst: February 26, 2007

DOI: 10.1007/s10973-005-7149-y